

Comparison of albedos computed by land surface models and evaluation against remotely sensed data

Xue Wei,¹ Andrea N. Hahmann,¹ Robert E. Dickinson,² Zong-Liang Yang,³ Xubin Zeng,¹ Kimberly J. Schaudt,⁴ Crystal B. Schaaf,⁵ Nicholas Strunell⁵

Abstract. The albedos of two land surface models, the Biosphere-Atmosphere Transfer Scheme (BATS) and the NCAR Land Surface Model (LSM), are compared with remotely sensed data and each other. The model albedos differ primarily because of their assumptions about and model differences in soil moisture content, soil color, snow albedo, shading of snow by canopy, and prescribed parameters for each land cover type. Global albedo maps for February and July 1995, developed from the advanced very high resolution radiometer (AVHRR) data, are used to evaluate model albedos. The models display a high bias as compared to the remotely sensed values in desert and semidesert regions. Over North Africa, LSM, whose albedos were previously tuned to data from the Earth Radiation Budget Experiment (ERBE), has the highest albedos. Elsewhere, and overall, BATS has the highest bias for desert and semidesert regions. Both models demonstrate a high bias over regions of winter snow, where the AVHRR data are expected to have a negative bias. LSM has especially high winter albedos, apparently because of intercepted snow increasing its canopy albedo.

1. Introduction

Albedo is defined as the ratio of the integrated total of reflected solar radiation to the integral of the incoming solar radiation [Monteith, 1973]. Land surface albedo directly controls the net solar radiation absorbed at the surface and thus the surface energy balance. Consequently, climate is sensitive to albedo variation and its changes by natural variations and human activities.

The climate response to changes in surface albedo has been a topic of considerable study. General circulation model (GCM) studies of the climate sensitivity to desertification [e.g., Charney *et al.*, 1977; Xue and Shukla, 1993] and tropical deforestation [e.g., Dickinson and Henderson-Sellers, 1988; Dirmeyer and Shukla, 1994; Hahmann and Dickinson, 1997] have largely involved the climate response to changes in a region's

surface albedo. Because of higher albedos, most such modeling studies have found the loss of radiative energy from the Amazon land surface to result in a reduction in convection and precipitation. A positive feedback mechanism may then be established with a reduction in vegetation cover due to the decrease in rainfall that could further enhance the albedo increase [Charney *et al.*, 1977; Dickinson and Hanson, 1984].

Errors in the specification of surface albedos in GCMs may also cause serious biases in surface temperatures such as those reported in the NCAR Community Climate Model version 3 (CCM3) by Bonan [1998]. High soil albedos in the Saharan region in this model caused temperatures that are several degrees (up to 5°C) colder than the observations throughout the year.

The derivation of a global albedo data set from surface information on land use type has been addressed by Matthews [1983, 1985] at 1° × 1° resolution for 32 surface types and by Clinton [1993]. The albedo associated with each different surface type has been derived from compilations of available surface-based reflectivity measurements. Hence the basis for including albedo at the land surface in climate models is still rather rudimentary, and based largely on a limited number of published surface observations. GCMs include variations of surface albedo with snow cover and soil moisture. Albedos are further related to climate variability through effects of agricultural planting and harvesting or land clearing, as well as drought and fires.

Climate model albedos and their connections to other climate variables can be further evaluated and improved

¹Institute of Atmospheric Physics, University of Arizona, Tucson, Arizona, USA.

²School of Earth and Atmospheric Sciences, Georgia Institute of Technology, Atlanta, Georgia, USA.

³Department of Hydrology and Water Resources, University of Arizona, Tucson, Arizona, USA.

⁴Department of Physics, University of Arizona, Tucson, Arizona, USA.

⁵Department of Geography and Center for Remote Sensing, Boston University, Boston, Massachusetts, USA.

Copyright 2001 by the American Geophysical Union.

Paper number 2001JD900218.
0148-0227/01/2001JD900218\$09.00

only through use of environmental satellite measurements. Pioneering studies to provide such global data sets include *Li and Garand* [1994], who used Earth Radiation Budget Experiment (ERBE) measurements to derive surface albedo ($2.5^\circ \times 2.5^\circ$) from top of atmosphere albedo, and *Csiszar and Gutman* [1999], who produced overhead surface albedos at 0.15° resolution from the advanced very high resolution radiometer (AVHRR) Global Area Coverage (GAC) data.

Although satellite observations are excellent at global mapping and monitoring of the distribution and variations of surface albedo, various factors complicate the retrieval of surface albedo from such measurements. Corrections are required for atmospheric absorption and scattering to estimate surface albedo from satellite measurements made above the atmosphere. Remotely sensed data depend on the view and solar angles (i.e., the surface is not Lambertian), and thus a bidirectional reflectance distribution function (BRDF) must be used to reconstruct the albedo. In addition, their radiances, sometimes made over narrow spectral bands, must be transformed to match the spectral bands used by climate models. Errors arise and accumulate at each of the above steps. Furthermore, the derivation of surface albedos is problematical over regions that may be either snow covered or cloudy because it is difficult to distinguish between these two possibilities. Because of such limitations, developing confidence in the use of such satellite-derived albedos in climate models requires comparisons of such albedos with those derived historically. Significant differences should be identified and explained.

The surface albedos calculated by two land surface models, the Biosphere-Atmosphere Transfer Scheme (BATS) [*Dickinson et al.*, 1993] and the Land Surface Model (LSM) [*Bonan*, 1996], which are coupled to a common GCM (the NCAR CCM3), are compared with the albedo derived from the advanced very high resolution radiometer (AVHRR) data. Section 2 briefly describes the computation of surface albedo by the two land surface models. The global albedo data set derived from AVHRR data is presented in section 3. Section 4 compares the albedo derived from remotely sensed data for the months of February and July 1995 with that computed by the land surface models and examines the annual variation of surface albedo computed by these two land surface models at several selected grid squares. Section 4 also provides further comparison between models and AVHRR data with area-averaged albedos for each different land cover type for the months of February and July. Section 5 summarizes our findings and presents our conclusions.

2. Model Albedo Computation

Land surface models such as BATS [*Dickinson et al.*, 1993] and LSM [*Bonan*, 1996] describe the processes occurring at the interface between the atmosphere and

the land surface. When coupled to a GCM, these models provide the input and the exchange of solar radiation, sensible heat, momentum, and latent heat fluxes. Both models use the current state of the atmosphere to force the land model, then use the calculated surface energy, constituent, and momentum fluxes to update the atmospheric conditions. A complete evaluation of the climate simulated by these models when coupled to CCM3 can be found in the works of *Hahmann and Dickinson* [2001] and *Yang et al.* [1999]. Both models use, in part, data from *Olson et al.* [1983] to derive surface types. Both are integrated with climatological sea surface temperatures (SSTs). In addition, a short integration was carried out with 1995 SSTs to explore possible boundary-condition-related differences between the 1995 and the long-term climate averages.

The time average model albedos are obtained by averaging the solar radiation reflected from the surface divided by solar radiation incident on the surface and not the average of instantaneous albedos. This quantity thus corresponds to the energy-weighted time average.

Each grid square in BATS is assigned one of 18 land cover types and one of 8 soil color classes, ranging from light to dark. An albedo for visible (wavelength less than $0.7 \mu\text{m}$) and near-infrared (wavelength greater than $0.7 \mu\text{m}$) radiation is then assigned to each land cover type and each soil color type. Only the moisture of its uppermost soil layer is used for soil albedo; however, a seasonally varying subsurface soil temperature is used for imposing a seasonality of vegetation properties and hence their effects on surface albedo.

LSM uses 12 basic plant functional types, which together with bare soil, are combined by fractional areas to constitute 28 different land surface types. Vegetation composition and fractional areas are time invariant. Time-varying leaf and stem areas, and their optical properties and time-invariant canopy heights and leaf dimensions, describe vegetation structure. There are nine soil color classes, the first eight of which correspond to those in BATS. The ninth class is a special class introduced to better match ERBE clear-sky albedos for desert and semidesert surface types located in North Africa and the Arabian Peninsula by increasing albedos from that of class 1 by 0.10. At each land grid cell, LSM can have up to five different surface types, including a fraction of lakes and wetlands. Vegetation albedos are computed using the two-stream approximation [*Sellers*, 1985].

The albedo of a grid box in either model is an average of three components: soil albedo, vegetation albedo, and snow albedo. That is,

$$\alpha = \alpha_s f_s + \alpha_{sn} f_{sn} + \alpha_v f_v, \quad (1)$$

where α stands for albedo and f stands for fraction, and the subscripts s , sn , and v refer to bare soil, snow, and vegetation, respectively. These three components are examined separately.

2.1. Soil Albedo

BATS and LSM have adopted the same formulation for soil albedo as a function of soil moisture and soil color but independent of solar zenith angle. The lighter the color, the higher is the soil albedo. They compute bare soil albedo α_s from

$$\alpha_s = \alpha_{s0} + 0.01 [\max(11 - 40S_{sw}/Z_u), 0], \quad (2)$$

where α_{s0} is the albedo for a saturated soil, S_{sw} is the surface soil water content, and Z_u is the upper soil layer depth. Therefore soil albedo becomes insensitive to increases in soil moisture when the depth of water in the upper layer is approximately 27.5% of the layer depth. Both models assume that the soil reflectance is isotropic for all incident solar angles. BATS prescribes saturated soil albedos for each color class and sets values of soil albedos for near-infrared radiation to twice that of the visible radiation. Over desert and semidesert regions, BATS increases soil albedos by 0.05 above the value computed by (2).

2.2. Snow Albedo

A number of previous studies have identified factors influencing snow albedo in BATS and LSM [Yang *et al.*, 1997, 1999; Yang and Niu, 2000]. The snow albedo in BATS depends on the solar zenith angle, grain size, and soot, as inferred from the albedo model of Wiscombe and Warren [1980], and the snow model and data of Anderson [1976], using a snow age parameter to provide the grain size and soot loading. The fractions of bare soil and vegetation covered by snow are represented by $f_{sn,s}$ and $f_{sn,v}$, respectively, both with the same function of snow depth and surface roughness.

$$f_{sn,s} = z_{snow} / (10 z_{0,s} + z_{snow}) \quad (3a)$$

$$f_{sn,v} = z_{snow} / (10 z_{0,v} + z_{snow}) \quad (3b)$$

where $z_{0,s}$ is the soil roughness (0.05m), $z_{0,v}$ is the roughness length for vegetation, and z_{snow} is snow depth in either case. These two fractions are then combined to determine the fraction of the grid square covered by snow (f_{sn}).

LSM bases its snow albedos on Marshall [1989]. Its snow albedo is a function of soot content (zero for Antarctica, 0.2×10^{-6} for Siberia, and 5×10^{-6} elsewhere) and zenith angle. The fraction of bare soil covered by snow is defined as

$$f_{sn,s} = \min(z_{snow}/z_{0,s}, 1). \quad (4)$$

By definition, $f_{sn,s}$ is always less than unity in BATS, but it can easily reach unity in LSM when the snow depth is higher than 5 cm. Thus, when snow accumulates, this difference tends to increase snow albedo at the soil surface faster in LSM than it does in BATS.

LSM, as BATS, considers the possibility that snow-pack may cover the vegetation by scaling the snow depth with the thickness of the canopy. However, this vertical burying is used to modify the amount of the effective leaves used in the radiative transfer calculation. In addition, LSM includes a snow effect neglected by BATS that appears to have a major impact on its calculation of wintertime forest albedos. New fallen snow tends to cover leaves and hence whiten a forest. LSM addresses this possibility by using its formulation of precipitation interception to cover its leaves during snowfall events. The formulation neglects possible removal of canopy snow by wind, and various other small-scale heterogeneities that could accelerate snow removal, and CCM3 may produce more frequent snowfall than would be realistic. Hence the LSM forest albedos could have a high wintertime bias. The LSM leaf fraction that is covered by intercepted water is defined in LSM in terms of the canopy water W_{can} , and the leaf and stem area indexes L and S :

$$f_{wet} = [W_{can}/p(L+S)]^{2/3}, \quad (5)$$

where p is a constant (0.1mm), and $p(L+S)$ represents the maximum water that can be held by the canopy. Because f_{wet} , which ranges from 0 to 1, does not depend on the roughness length of LSM vegetation, it increases over forests much more rapidly with snowfall compared with $f_{sn,v}$ in BATS, significantly increasing their albedos. The leaf fraction that is covered by intercepted snow computed using (5) modifies the vegetation optical parameters used in the two-stream approximation [Sellers, 1985].

The snow albedo of BATS is a function of solar angle only when the Sun is close to the horizon, whereas that of LSM is much more sensitive to solar angle change. The snow albedo of BATS is only indirectly affected by temperature through the temperature dependence of the grain size growth rate. The snow albedo of LSM, however, is directly decreased by the ground temperature warming. Consequently, the albedo of BATS for fresh snow is generally substantially larger than that of LSM and appears to remain larger than that of LSM with ageing everywhere except for the Siberian region (cf. Yang and Niu [2000], figure 6).

2.3. Vegetation Albedo

The BATS model prescribes a diffuse albedo for each plant cover type for two spectral bands. The direct Sun albedos are obtained from the diffuse values by the solar angle dependence as a function of plant type that consequently imposes a seasonal and a diurnal variation. The fraction of vegetation changes with season through its dependence on subsurface temperature.

LSM obtains its canopy albedos through its prescription of plant-type-dependent leaf reflectance and transmittance and through leaf orientation. These parameters are combined with soil albedo, seasonally vary-

ing leaf area index (LAI), and solar angle through use of the two-stream approximation [Sellers, 1985]. The fraction of vegetation is fixed for each land cover type. The LSM surface albedo becomes insensitive to ground albedo when LAI is larger than 2, at which point the leaves shade most of the ground. Vegetation albedos are the lowest when the Sun is at nadir. The dependence on solar angle becomes stronger with increasing LAI. Because of their greater interception of light, horizontal leaves give a larger canopy albedo than vertical ones at nadir.

3. Remotely Sensed Albedo Data

Strugnell and Lucht [2001] derived global albedos from channels 1 (580–680 nm) and 2 (725–1100 nm) of the NOAA-14 AVHRR sensor data for the months of February and July 1995, at a 10 km horizontal resolution. These are compared to model albedos by simply averaging all 10 km values within each model grid square (approximately $2.8^\circ \times 2.8^\circ$) over land.

Strugnell and Lucht [2001] employed the Ross Thick Li Sparse Reciprocal (RTLSR) model [Ross, 1981; Li and Strahler, 1992; Roujean et al., 1992; Wanner et al., 1995; Lucht et al., 2000]. With sufficient observation at multiple solar zenith angles, the RTLSR model can be used to fit a BRDF to the measured bidirectional reflectance factors (BRFs). When the BRDF is sparsely sampled, however, its estimation is improved by assuming *a priori* knowledge of underlying surface BRDF guided by a land cover classification. Theory and measurements suggest that groupings of land covers will have similar BRDFs. Thus, intraclass BRDFs are broadly similar and differ more in magnitude than in the shape of the BRDF function. A family of BRDFs is defined by *Strugnell et al.* [2001] as a group of land cover classes that have similar BRDFs:

$$F_n = \beta f_n(\vec{\Omega}_i; \vec{\Omega}_r), \quad 0 < \beta < 1/\rho_{l,ws}, \quad (6)$$

where F_n represents the family of BRDFs associated with land cover type n and $f_n(\vec{\Omega}_i; \vec{\Omega}_r)$ is a typical BRDF for that land cover type, $\vec{\Omega}$ is the direction vector, and the subscripts i and r represent incident and reflected directions, respectively, β is a scaling factor, and $\rho_{l,ws}$ is the diffuse component of the albedo associated with $f_n(\vec{\Omega}_i; \vec{\Omega}_r)$. Although β is theoretically constrained to insure that no albedos exceed 1., it should also remain close to unity; otherwise, the assumption that members of a BRDF family have similar shapes is suspect because of the likelihood of different radiation scattering mechanisms. This use of a scaling factor dramatically improves the retrieval estimates of albedo compared to assigning the same BRDF for all pixels of a certain land cover.

The time-invariant global land classification used here to assign BRDF shapes is that of *Olson* [1994], as ob-

tained from AVHRR 1 km data by *Loveland et al.* [2000]. The Olson land-cover types are divided into three groups: discrete canopies, where individual crowns in the canopy have a shadow-casting effect; layered canopies, where the canopy is continuous and dominated by volume scattering; and backgrounds. Seasonal growth and senescence of vegetation will change the scattering characteristics of the canopy. For this reason, different look-up tables were constructed for summer and for winter, both with and without a snowy background.

Strugnell and Lucht [2001] estimate the surface reflectance spectrum by fitting a laboratory-measured spectrum to a linear combination of those observed channels 1 and 2 reflectances of the NOAA-14 AVHRR bands (580–680 nm and 725–1100 nm, respectively). They use the bottom of the atmosphere solar irradiance spectrum for the energy weights needed to compute albedo over any particular spectral integral. The initial AVHRR data were atmospherically corrected only for Rayleigh scattering and ozone absorption. For the albedo estimates, a small additional aerosol correction was applied to the data assuming a standard U. S. continental atmosphere (i.e., a constant aerosol optical depth of 0.15 at 550 nm) using the 6S program [Vermote et al., 1997].

Persistent cloud cover and excessive amounts of atmospheric aerosols, such as those derived from biomass burning, can contaminate the surface albedo retrieval and should be minimized. Therefore the 1 km AVHRR imagery was used in the form of a 10-day maximum normalized difference vegetation index (NDVI) reflectance value as composites for February (winter) and July (summer) 1995. Three consecutive 10-day composites were further composited to eliminate cloud cover in some areas, such as the mountainous regions of Central America. Since clouds have albedo values similar to those of snow, such a cloud-minimization scheme also minimizes the number of snow-covered pixels in the scene by choosing snow-free pixels over snow-covered ones. Thus areas shown as snow-covered are only those that are snow covered for every day of the month in question. The retrievals of albedo over snow-covered areas should therefore be treated with caution.

Global albedo data sets were derived for July and February 1995 using the above procedures. In the absence of any other independent sources of data, *Strugnell and Lucht* [2001] estimated the overall errors of their surface albedo retrieval as the combined error of each of the steps of their algorithm (i.e., errors in aerosol optical depth, BRDF inversion algorithm, and broadband conversion). This procedure estimates albedo errors of 29%, 11%, and 13% for visible albedo, near-infrared (NIR) albedo, and total shortwave, respectively. Relative errors such as these equate to absolute errors in the visible, which are of the order of ± 0.015 . Typical absolute errors in NIR and total shortwave are ± 0.03 .

4. Model Albedos Over Land

4.1. Global Distribution

The global albedo distribution and global differences among the models and remotely sensed data are evaluated for the months of February and July, corresponding to the two months for which AVHRR albedos were derived.

The comparison of July and February albedos between the two models is presented in Plate 1. In July, Plate 1b shows that BATS has higher albedos than LSM in many desert and semidesert regions, by as much as 0.1 in central Australia, the southern corner of South America, central Asia, South Africa, and some parts of North America. However, over northern Africa, where LSM has increased its albedo by 0.1 to obtain better agreement with ERBE, it gives substantially higher values than BATS. Similar differences are seen in the February albedos (Plate 1d).

The February comparison also shows large differences in regions usually with substantial snow cover, such as North America and Russia. The higher values of LSM, by up to 0.1, are most likely a combined result of its canopy snow interception and high tendency to reach unity in its ground snow cover fraction, since the BATS albedos for bare snow tend to be larger than those of LSM [Yang and Niu, 2000].

Compared to remotely sensed data, both models show higher albedos than observations over desert and semidesert in July and February (Plate 2). Where BATS has higher albedo than LSM (Plates 1b and 1d), its excess over the AVHRR estimate is in the range of 0.1 to 0.2 (Plates 2b and 2d). Over the North African region, LSM is similarly high and BATS closer to the AVHRR albedos. In the Saharan region, the AVHRR values of lower than 0.4 are less than values given by airborne measurements of surface albedo over northwestern Sahara, which had a mean of 0.43 and a standard deviation of 0.021 [Barker and Davies, 1989; Rockwood and Cox, 1978].

Over tropical South America, LSM albedo is very close to observations, while the BATS albedo is slightly lower than that observed (0.02–0.05), and increasingly so for Central America. Over the Sahel region (15°N), on the margin of the northern African desert, BATS has a line of grid squares with albedos that are low compared to those shown by AVHRR. Both models have classified most of these squares as grassland. According to Tucker *et al.* [1985] the land cover type for this region corresponds to wooded grassland and bushland. The original geographic information going into the land cover classification used by BATS and LSM could be quite old, and the discrepancy could, in part, reflect changing land use or shifts in the land affected by aridity. It could also be some artifact of the averaging used to provide the GCM albedo information or of their fail-

ure to account for differences in grassland albedos, with the Sahel grassland being unusually high in albedo because of lower LAI and brighter soil than allowed for. In addition, unusually high precipitation that year could have lowered albedos from those of previous years that suffered from long-term drought.

In the central part of North America and most of Asia and Europe, BATS albedos are in closer correspondence to those of AVHRR than those of LSM. For February, Plate 2d shows BATS albedos to be much higher than those from AVHRR over regions of North America and Eurasia which are expected to be snow covered. Large positive biases occur between model simulated and observed albedos over the Himalayas and western China (Plate 2d). The year 1995 was anomalously warm over all of northern Asia, with large positive temperature anomalies (4°–6°) over north central and northeastern Asia [National Oceanic and Atmospheric Administration (NOAA), 1995]. The snow cover, hence the observed albedo, could consequently have been anomalously low. However, the model-simulated temperatures in this region are also above the observed average conditions [Bonan, 1998]. The simulations with 1995 SSTs showed little or no differences in albedo from the long-term simulation, *i.e.*, much smaller in magnitude than the differences between model and observations.

4.2. Seasonal Variation of Model Albedos

Six land cover types (represented by six model grid boxes), whose combined areas occupy over half of the global land area, are chosen to examine the seasonal variation of model albedos. The geographical location, land cover type, and soil classification of these six grid boxes are listed in Table 1.

4.2.1. Broadleaf evergreen trees (BETs), Figure 1. The grid box that represents the broadleaf evergreen trees (BETs) is located in the Amazon. The albedo of BATS is smaller than that of LSM and has a larger seasonal variation (Figure 1a); the two models differ by as much as 0.025 (*i.e.*, 20%) during the wet season (from December to April), with the smallest differences in July. BATS assumes a smaller near-infrared (NIR) albedo than that given by LSM, but the visible albedos are about the same. Since the vegetation fraction of BATS remains constant (0.9) through the year for broadleaf evergreen trees, it does not contribute to albedo changes. Hence its seasonal changes in albedo are controlled mainly by soil moisture variations over the 10% of the box covered by bare soil (Figure 1b).

LSM assumes that all the properties of broadleaf evergreen trees affecting albedo, such as LAI, are constant throughout the year. Furthermore, the LSM fraction of bare soil is only 5%, so changes of the soil albedo will have less effect on the grid box albedo than they do on BATS (Figures 1a and 1b). The only other seasonal

Table 1. Location, Vegetation Type, and Soil Classification of Grid Boxes Chosen to Study the Annual Variation of Albedo.

BATS Land Cover Type	Center Latitude/ Longitude	Geographic Region	Soil Color Type
Broadleaf evergreen tree (BET)	7.0°S, 61.9°W	Amazon	4
Needleleaf evergreen tree (NET)	57.2°N, 101.3°W	Canada	4
Tundra (TUN)	62.8°N, 146.3°W	northern Canada	4
Desert (DES)	29.2°S, 126.6°E	Australia	1 (BATS) 2 (LSM)
Grass (GRS)	23.5°N, 101.3°W	Mexico	6
Evergreen shrub (EGS)	26.5°S, 146.3°E	Australia	2

variations that might explain the very small seasonal variations in albedo of LSM are those related to the solar angle.

Culf et al. [1995] studied the seasonal variation of albedo in this region and suggested that the seasonal variation of albedo over the Amazon tropical forest is mostly driven by changes in soil moisture. Observational studies [*Oguntoyinbo*, 1970; *Pinker et al.*, 1980; *Shuttleworth et al.*, 1984] over tropical evergreen forests agree on a surface albedo of about 0.13. Both models are also near this value. The seasonality of the BATS albedo is a plausible response to the seasonality of precipitation.

4.2.2. Needleleaf evergreen trees (NETs), Figure 2. For the needleleaf evergreen trees (NETs) box in Canada, BATS has a higher albedo in summer but lower albedo in winter than LSM (Figure 2a). The vegetation fraction in BATS implies soil fractions varying from 20% in midsummer to 30% from November to May. Snow is a major factor in determining the winter albedos of this high-latitude location. Snow is absent in summer, when albedos are low, but from December to May, it nearly covers all the bare soil (Figure 2b). Snow also covers about 10% of the vegetation. Overall, snow imposes its large albedo on about 40% of the surface.

At the same point but for LSM, needleleaf evergreen trees cover 75% of the grid square with the rest being bare soil. Because at this point the LAI is greater than 4., the albedo changes little with changes in LAI and ground albedo. Hence the LSM seasonal albedo variation is also determined mostly by changes in snow cover. LSM generally assigns lower albedos for snow-free needleleaf trees than does BATS. However, because BATS only piles snow on top of vegetation that is shorter than the depth of the snow pack, whereas LSM piles any snow that falls on its leaves, its needleleaves are much more easily covered by wintertime snow than are those of BATS. In addition, the soil surface is also more easily covered by snow in LSM than in

BATS. Therefore in BATS, snow contributes less to the grid square albedo, and it has lower albedo in winter. This feature is apparent in the global distribution of February albedo differences between these two models (BATS-LSM, Plate 1d) where large negative differences are found in northern North America and Siberia.

We use the ground measurements taken in the Boreal Ecosystem-Atmosphere Study (BOREAS) at seven conifer sites in 1994 and 1995 [*Betts and Ball*, 1997] to further evaluate albedo over the boreal forest. The BOREAS data in February and July give mean albedo values of 0.13 and 0.08 compared to the AVHRR values of 0.11 and 0.12 for the same location and months. Consequently, AVHRR may underestimate boreal forest albedos in winter but possibly not by enough to make the climate model winter albedos plausible and, if anything, may be an overestimate in summer. All the BOREAS measurements suggest low albedos for the boreal forest in winter, generally in the range 0.10–0.20, and rarely as high as 0.30. Hence the winter boreal forest albedos of around 0.35 in LSM and 0.31 in BATS are likely to be excessive. In general, the albedos for both models have high biases, especially LSM in winter and BATS in summer.

4.2.3. Tundra (TUN), Figure 3. The albedos of the two models at the tundra (TUN) grid box in northern Canada are very similar from July to March (Figure 3a) but differ significantly during the snowmelt season. The BATS vegetation fraction varies between 40% and 50%, and in winter both vegetation and bare soils are largely covered by snow (Figure 3b) and hence have high albedos. In summer, both soil and vegetation contribute to the albedo. LSM assigns a vegetated fraction of 60% that is comprised of two plant cover types: arctic grass and arctic deciduous shrub. Their LAIs are close to zero in winter, allowing the underlying snow to dominate the surface albedo. The physical processes responsible for albedo changes are similar to those in BATS.

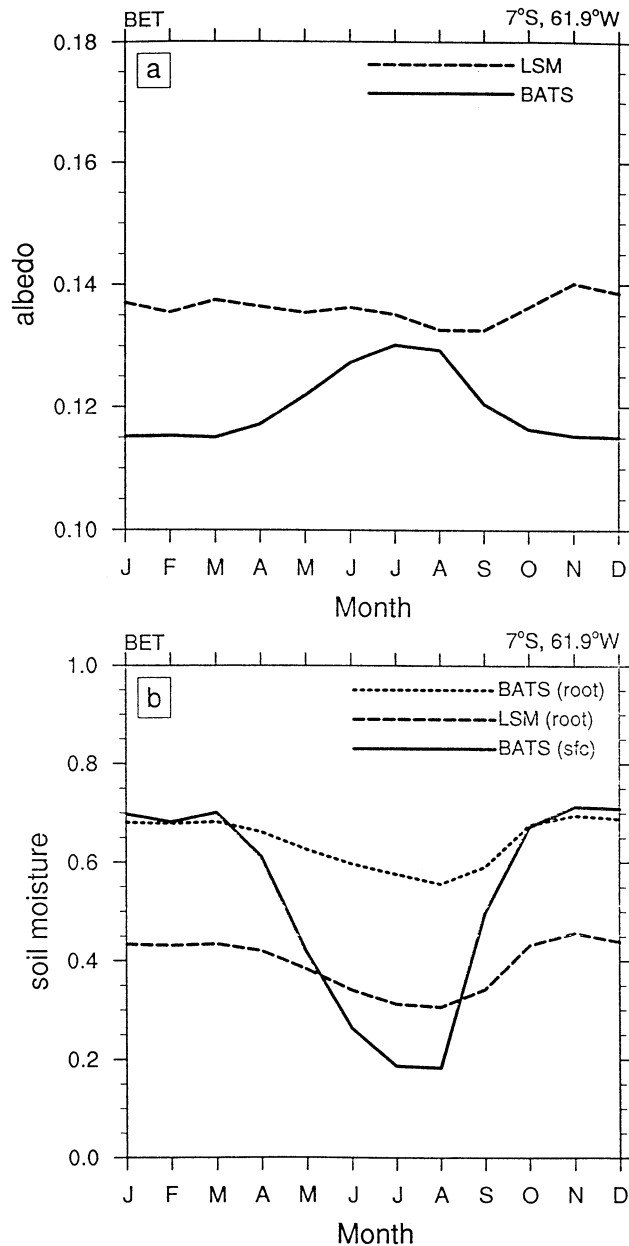


Figure 1. Annual distribution in model-simulated (a) total surface albedo (BATS and LSM), (b) upper layer and root-zone soil moisture ratio (BATS) and root-zone volumetric soil water (LSM) for a broadleaf evergreen tree (BET) grid square.

The albedo from LSM is remarkably lower than that from BATS during the snowmelt season (April–June). The albedos in LSM are parameterized to be lower as the grid point temperatures approach those of melting (Figure 3c). Albedos are further decreased in LSM compared to BATS when snow begins to melt. Snow in LSM disappears one month earlier than in BATS, a result consistent with earlier studies [Yang and Niu, 2000].

4.2.4. Desert (DES), Figure 4. Desert albedo is calculated in both models by (2) and in BATS increased by 0.05 beyond that. For the desert grid square (DES) in Australia, soil color class classification is 1 in BATS

and 2 in LSM. In BATS the seasonal variation in albedo (Figure 4a) is evidently a result of the seasonality of soil moisture (Figure 4b), as seen in the inverted patterns between these two quantities. On the other hand, both albedo and soil moisture in LSM, as indicated by their rooting zone values (Figure 4b), remain almost constant throughout the year. The soil color class is 1 for all desert and semidesert points in BATS, while LSM soil color classes range from light to dark (1–9). The albedo difference between soil colors 1 and 2 is at most about 0.02. Therefore the 0.05 to 0.10 higher albedos of BATS must be a result of drier soils (although the root zone

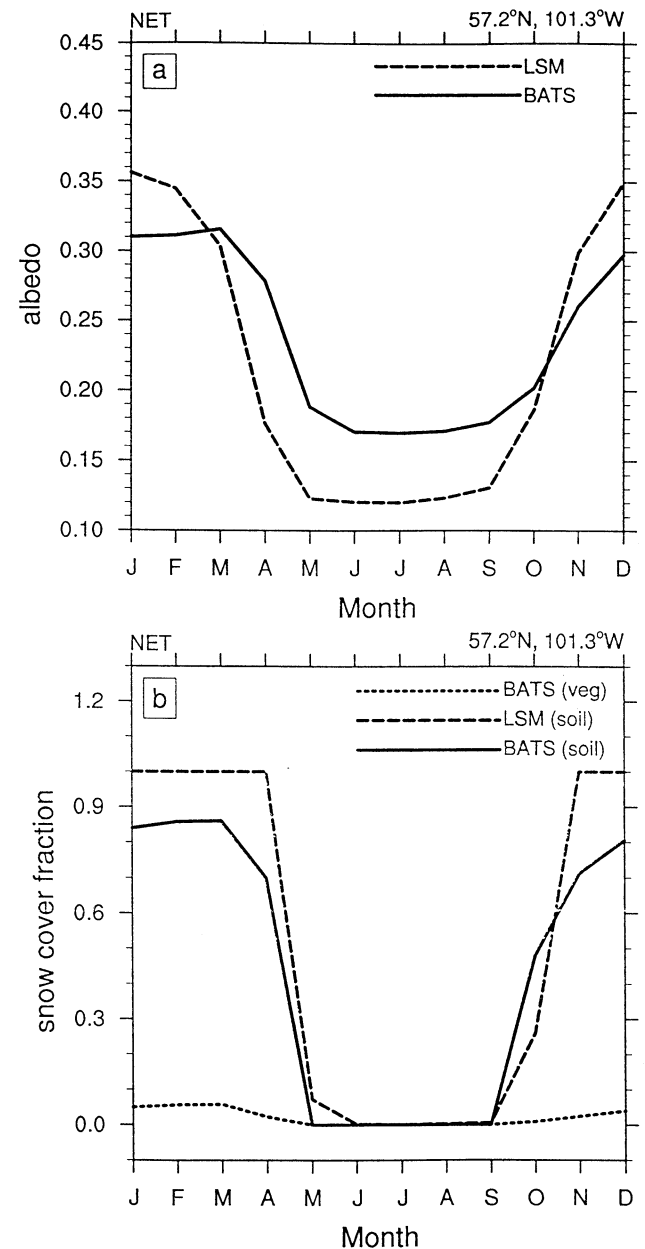


Figure 2. Annual distribution in model-simulated (a) total surface albedo (BATS and LSM), (b) fraction of bare soil covered by snow (BATS and LSM), and fraction of the vegetation covered by snow (BATS) for a needleleaf evergreen tree (NET) grid square.

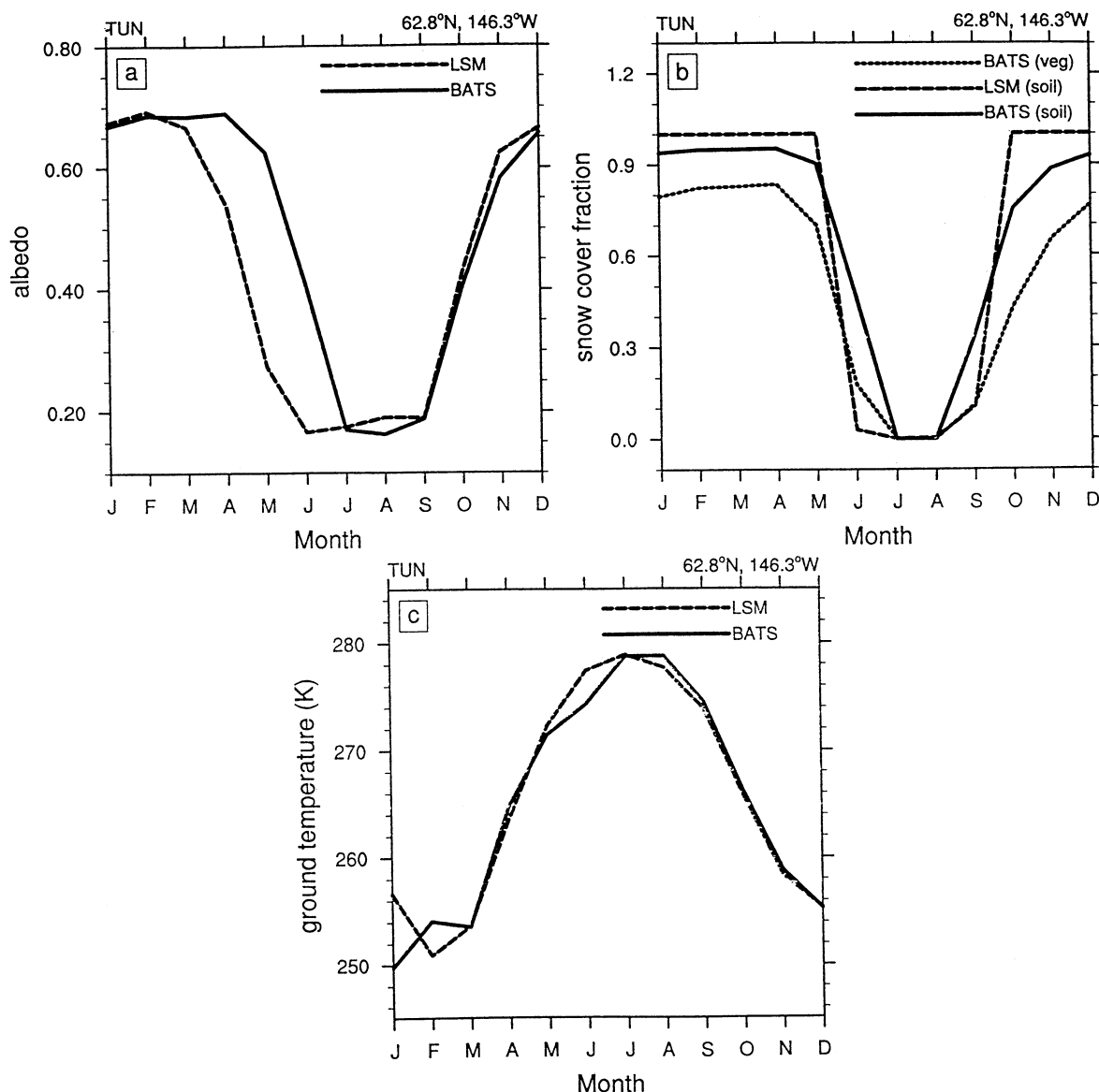


Figure 3. Annual distribution in model-simulated (a) total surface albedo (BATS and LSM), (b) fraction of bare soil covered by snow (BATS and LSM), fraction of the vegetation covered by snow (BATS), and (c) ground temperature (K, BATS and LSM) for a tundra (TUN) grid square.

soil moisture content is smaller in LSM than in BATS). Indeed, the upper layer moisture in BATS is drier than that of LSM (not shown) for most of the year.

For regions with little vegetation, much of the underlying soil is exposed to direct solar irradiance and sensor viewing. The strong anisotropic scattering properties of actual soil depend on solar angle and view angle. Consequently, the assumption of isotropic albedos may limit the performance of the models.

4.2.5. Grass (GRS), Figure 5. The grass cover (GRS) box located in Mexico is examined. The albedo of grass in BATS is around 0.20 and bare soil in the range of 0.13 to 0.18, depending on soil moisture, which covers 20%–25% of the surface. BATS visible albedos are smaller than those of LSM, but the near-infrared values are larger. Soil total albedos remain near those of grass, and the vegetation fraction varies little, so BATS

has a negligible seasonal variation. LSM albedo has a more pronounced seasonal variation, from 0.175 in February to 0.235 in August, as the soil and grass albedos vary in phase (Figure 5a). The soil is wettest from January to March and driest from August to November (Figure 5b), whereas the prescribed LAI and soil area index (SAI) vary from near-zero values from September to April to values larger than 3 and 2, respectively, by the beginning of August. Thus the lowest LSM albedo of about 0.175 results in the wintertime, from low values of LAI underlain by a dark wet soil. The highest LSM albedos occur in summer when the soil brightens because of its dryness and the leaves, and especially stems, contribute to higher albedos. A model with growth of grass coupled to soil moisture might provide a rather different seasonality at this location.

There have been a few reported studies concerning

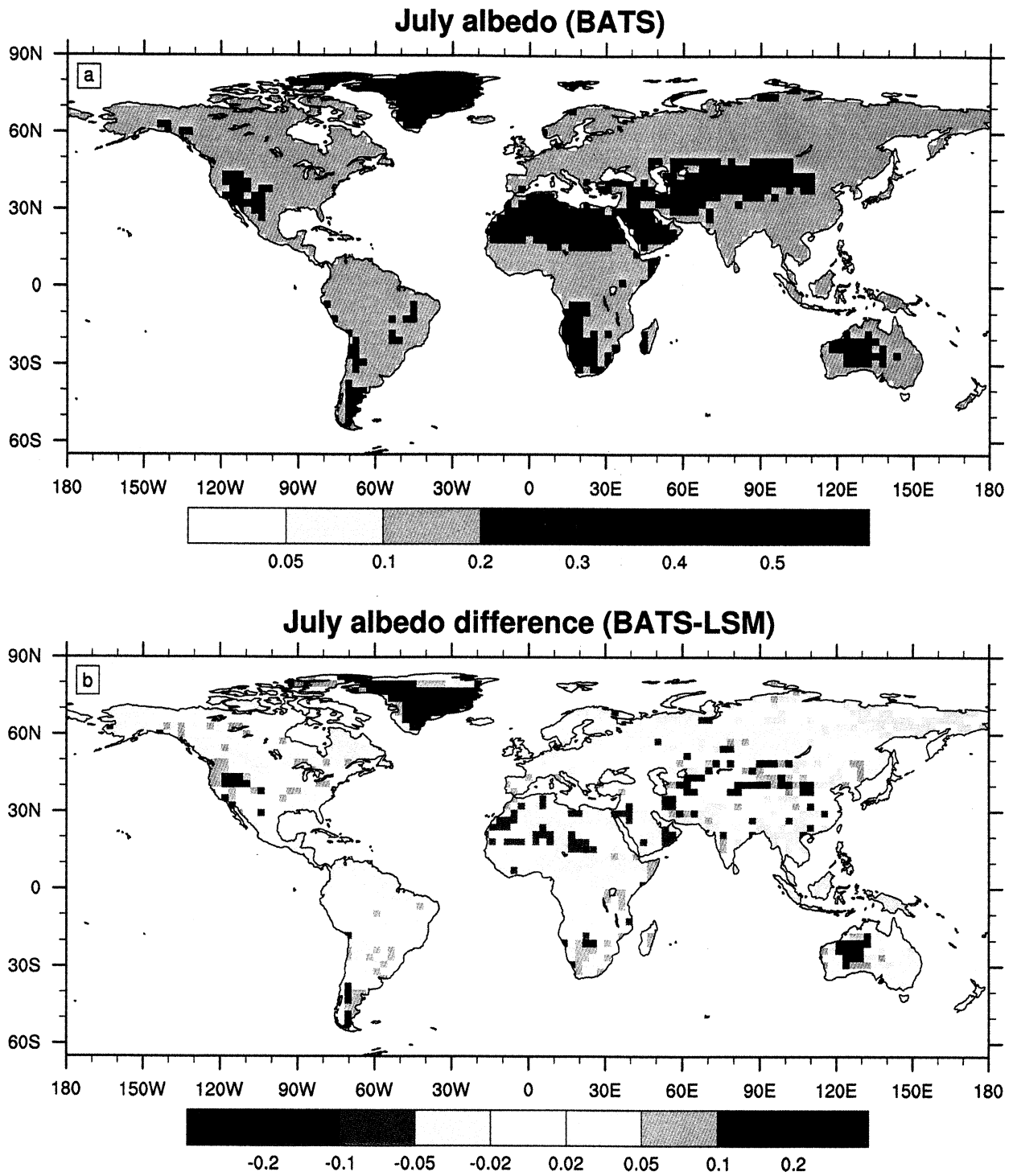


Plate 1. Geographic distribution of model-simulated land surface albedo: (a) July CCM3-BATS, (b) July differences (CCM3-BATS - CCM3-LSM), (c) February CCM3-BATS, and (d) February differences (CCM3-BATS - CCM3-LSM).

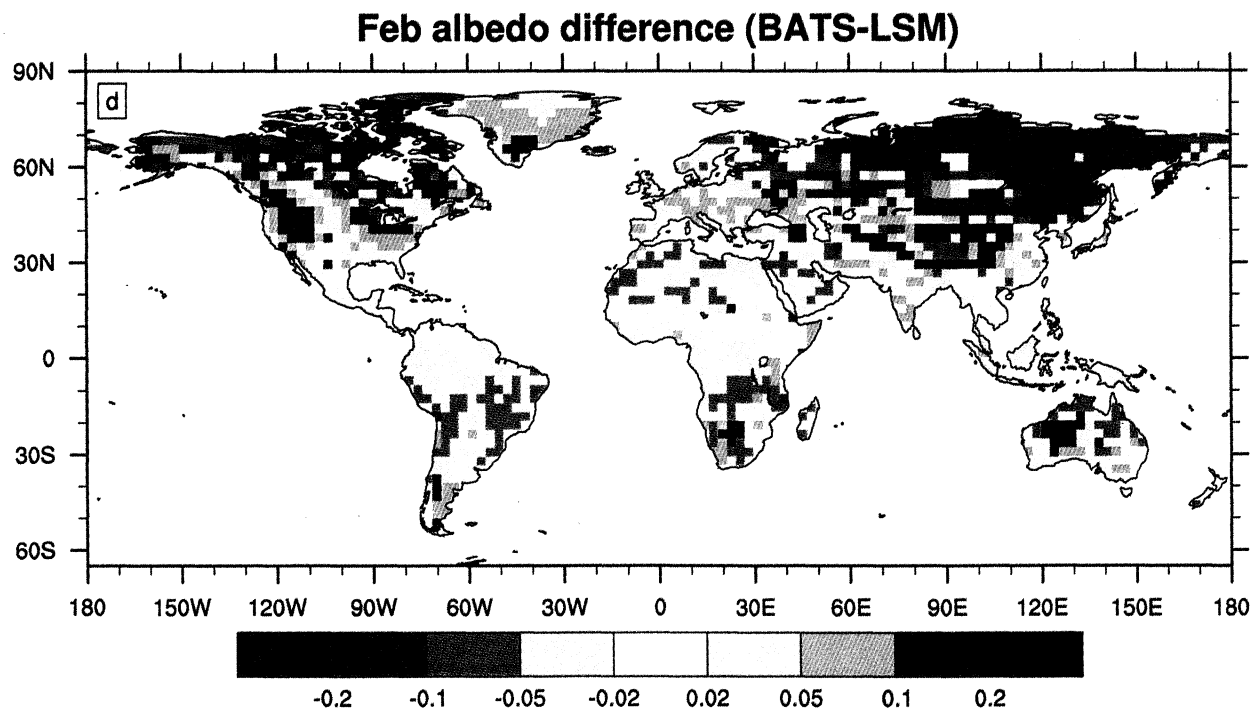
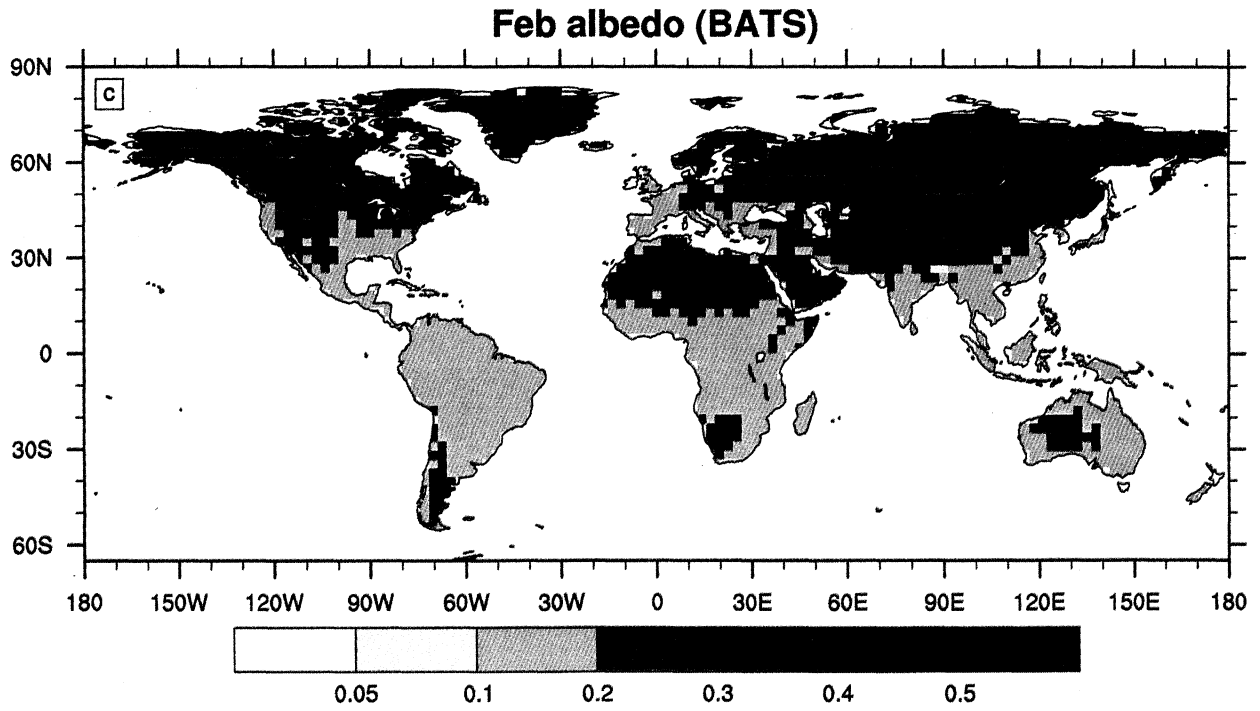


Plate 1. (continued)

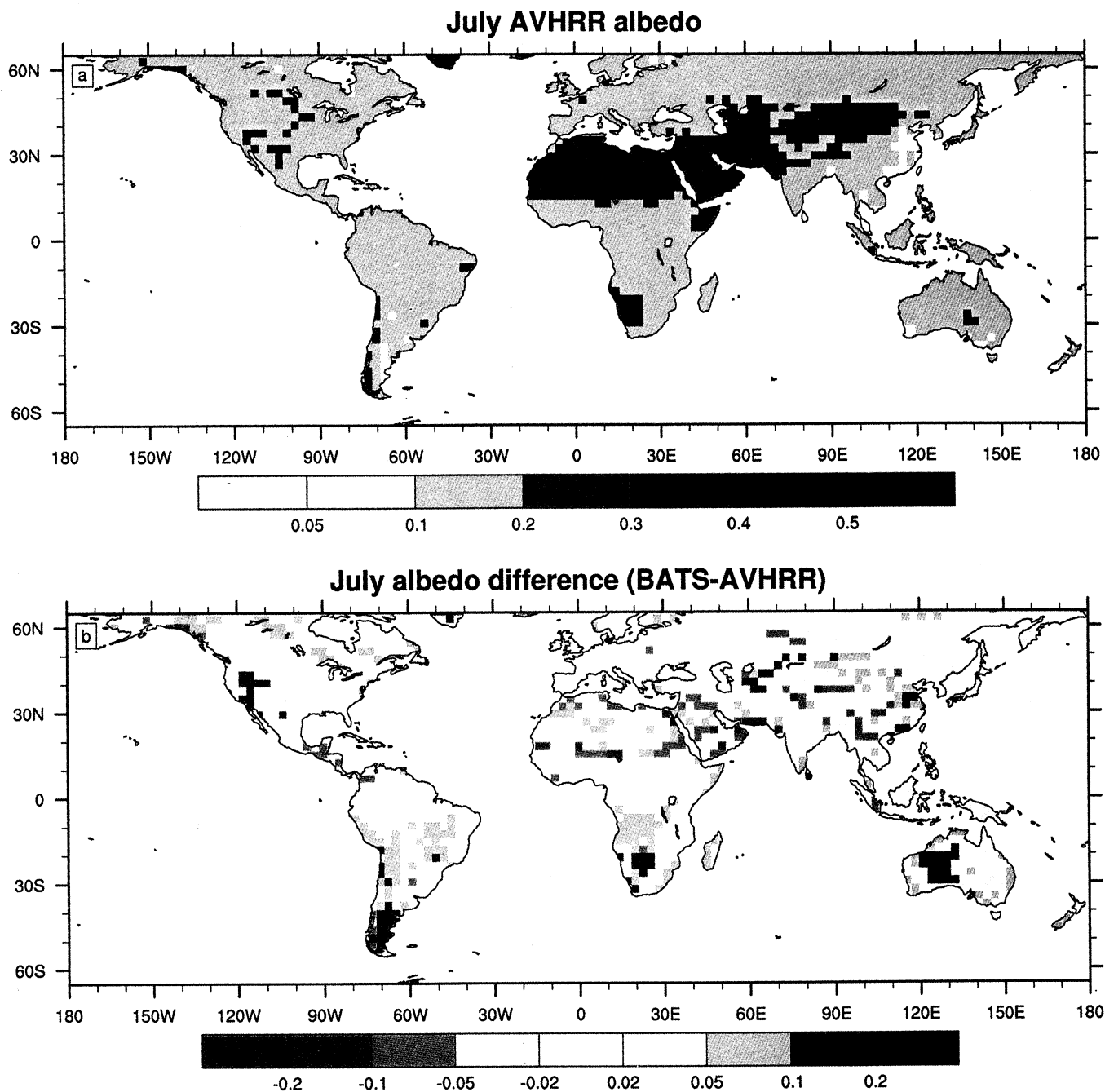


Plate 2. Geographic distribution of land surface albedo: (a) satellite-derived (AVHRR) for July 1995, (b) July differences between AVHRR-derived albedos and that simulated by CCM3-BATS, (c) AVHRR for February 1995, and (d) the February differences between AVHRR-derived albedos and that simulated by CCM3-BATS.

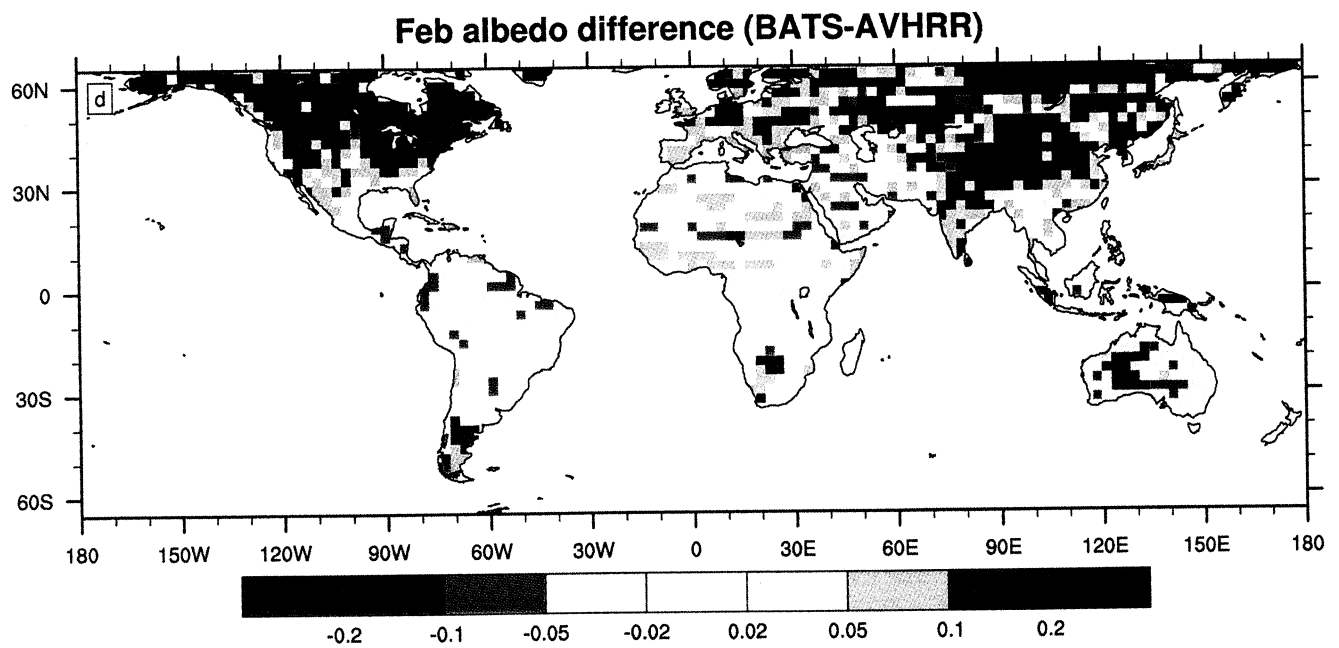
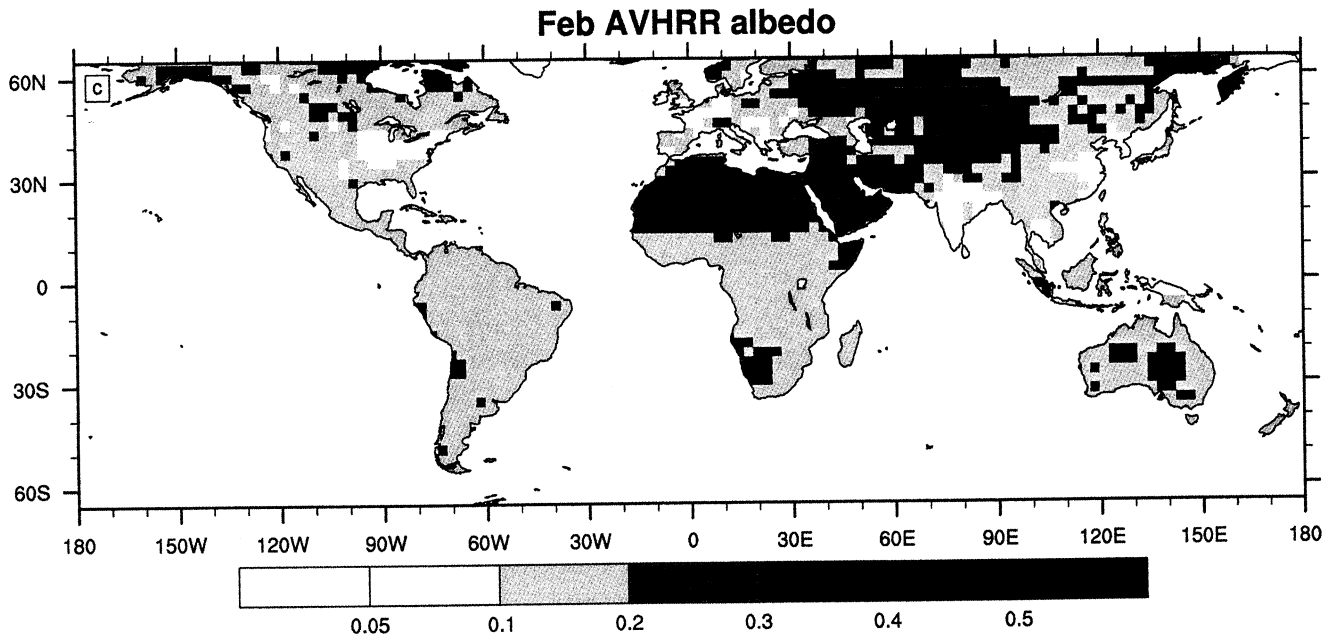


Plate 2. (continued).

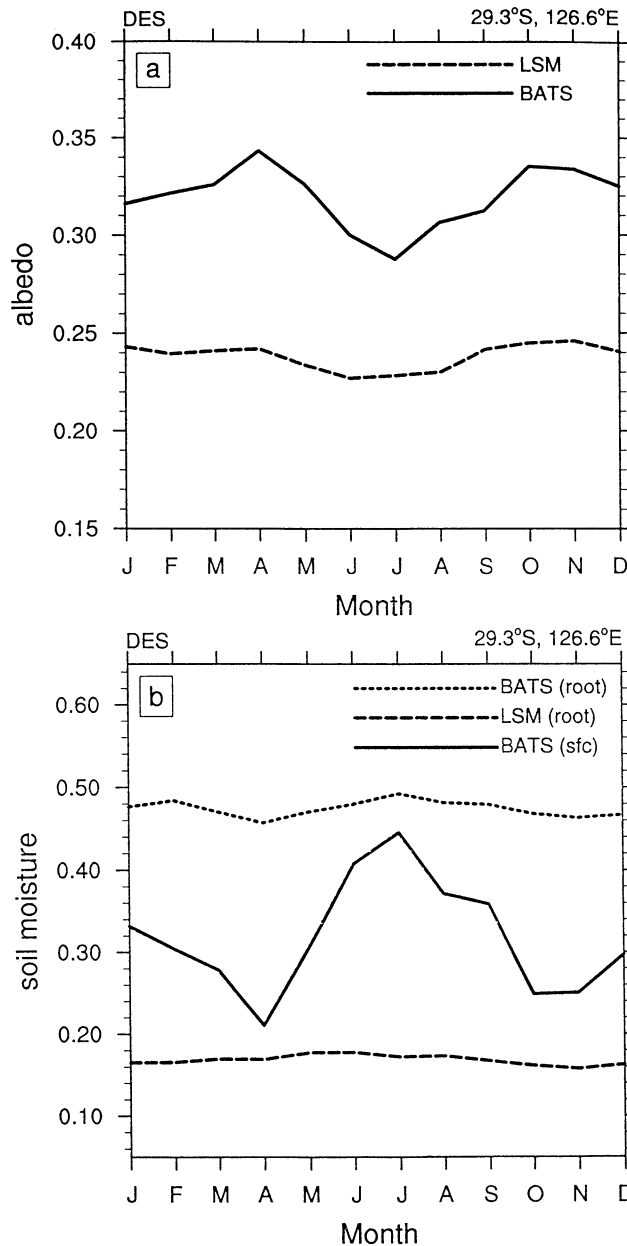


Figure 4. Annual distribution in model-simulated (a) total surface albedo (BATS and LSM), (b) upper layer and root-zone soil moisture ratio (BATS), and root-zone volumetric soil water (LSM) for a desert (DES) grid square.

the albedo of tropical grasslands. *Oguntoyinbo* [1970] studied a variety of natural and agricultural surfaces in Nigeria and found seasonally varying grass albedos ranging from 0.16 to 0.25. *Pinker et al.* [1980] measured seasonally varying values for grass in tropical forest clearings in Thailand, ranging from 0.13 to 0.16. More recently, *Bastable et al.* [1993], in central Amazonia, measured an albedo of 0.16 for grass ranchland at the end of the dry season. AVHRR data show grassland albedo as low as 0.05 and as high as 0.3. Burning can cause very low albedo because black ashes cover the ground; grazing and soil moisture reductions can lead to higher albedo. Hence the wide range of grass albedos

indicated by the AVHRR data for different places and times, but not the models, may be realistic.

4.2.6. Evergreen shrub (EGS). At the shrub (EGS) box, located in Australia, the vegetation fraction of BATS varies between 0.7 and 0.8. Shrub albedo is about 0.14, and soil albedo varies between 0.21 and 0.24. Hence the surface albedo in BATS varies from 0.15 in summer to 0.17 in winter, as the bare fraction increases in response to colder temperatures. In LSM, 80% of the grid box is covered by shrubs with albedo of about 0.119 and 20% with bare soil. The significantly lower shrub albedos give this location in LSM a lower year-round albedo than that of BATS.

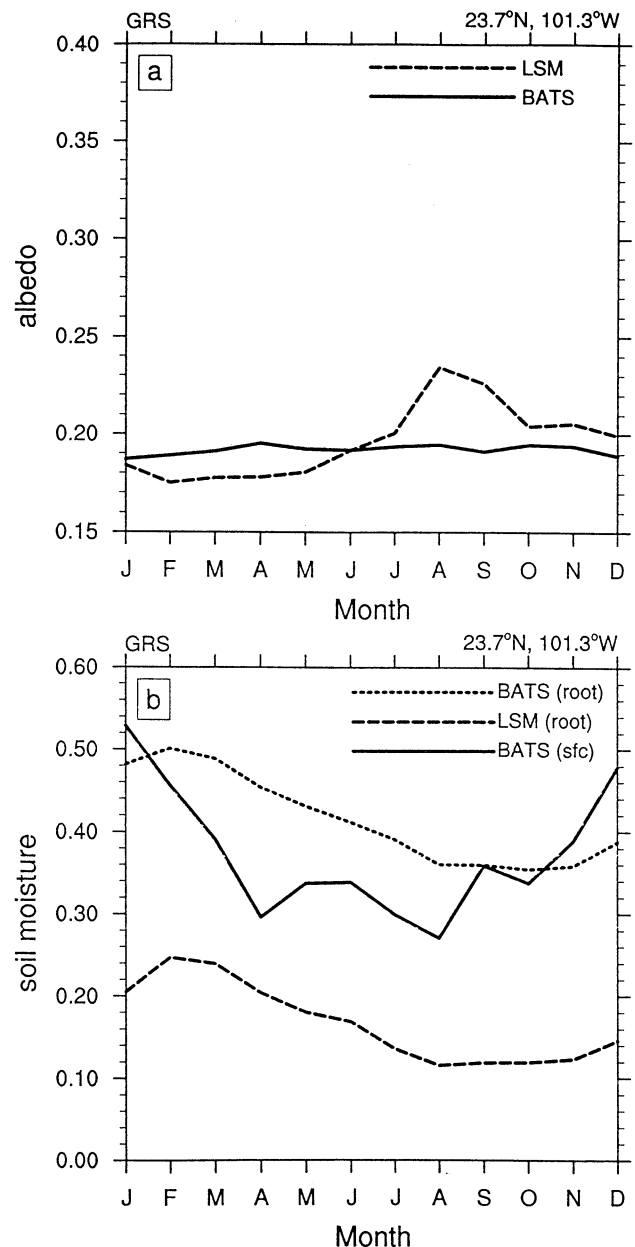


Figure 5. Annual distribution in model-simulated (a) total surface albedo (BATS and LSM), (b) upper layer and root-zone soil moisture ratio (BATS), and root-zone volumetric soil water (LSM) for a grassland (GRS) grid square.

Table 2. Area-Averaged Monthly Surface Albedo for 11 Land Cover Types From Models (BATS and LSM) and AVHRR ^a

Land Cover Type	Month	Area Covered ($\times 10^6 \text{ km}^2$)	BATS Albedo	LSM Albedo	AVHRR Satellite Albedo
Broadleaf evergreen tree	Jul	14.6	0.119(± 0.008)	0.139(± 0.010)	0.142(± 0.020)
	Feb	13.8	0.116(± 0.005)	0.139(± 0.013)	0.143(± 0.036)
Needleleaf evergreen tree	Jul	10.0	0.146(± 0.013)	0.120(± 0.031)	0.132(± 0.020)
Tundra	Jul	9.2	0.187(± 0.081)	0.188(± 0.038)	0.173(± 0.079)
Desert and semidesert	Jul	16.0	0.330(± 0.042)	0.316(± 0.099)	0.280(± 0.078)
	Feb	6.3	0.326(± 0.056)	0.258(± 0.090)	0.237(± 0.064)
Short grass	Jul	20.8	0.197(± 0.013)	0.206(± 0.021)	0.199(± 0.049)
	Feb	10.5	0.193(± 0.015)	0.229(± 0.029)	0.187(± 0.042)
Broadleaf deciduous tree	Jul	5.2	0.176(± 0.015)	0.167(± 0.032)	0.152(± 0.023)
	Feb	4.3	0.170(± 0.010)	0.211(± 0.031)	0.152(± 0.020)
Needleleaf deciduous tree	Jul	5.7	0.138(± 0.006)	0.137(± 0.024)	0.137(± 0.021)
Crop	Jul	10.7	0.186(± 0.009)	0.180(± 0.020)	0.168(± 0.030)
	Feb	3.3	0.185(± 0.008)	0.165(± 0.032)	0.150(± 0.038)
Tall grass	Jul	9.7	0.181(± 0.013)	0.177(± 0.027)	0.155(± 0.023)
	Feb	8.2	0.182(± 0.013)	0.182(± 0.034)	0.155(± 0.023)
Deciduous shrub	Jul	3.6	0.180(± 0.020)	0.164(± 0.039)	0.187(± 0.058)
	Feb	3.6	0.179(± 0.014)	0.142(± 0.024)	0.185(± 0.052)
Evergreen shrub	Jul	1.7	0.152(± 0.012)	0.123(± 0.034)	0.162(± 0.031)
	Feb	2.8	0.150(± 0.009)	0.117(± 0.024)	0.184(± 0.018)

^a Averaged values are from 90°N to 20°S in July and from 90°S to 20°N in February.

4.3. Remotely Sensed Albedo Within the Same Vegetation Types

To complement the map and single location comparisons, Table 2 compares area-averaged albedos according to land cover type. To avoid complications in the interpretation of snow-covered areas, we have averaged points from 90°N to 20°S in July and from 90°S to 20°N in February. Grid squares, in both models and observations, are grouped according to the BATS classification for land cover types. This table also provides an estimate of the spatial variability of these albedos through their standard deviation.

Several of our earlier conclusions are further supported. In particular, both models are in reasonable agreement with AVHRR for broadleaf evergreen albedos except that BATS albedos are low by about 0.02. *Culf et al.* [1995] observed the albedos of tropical forest for 4 continuous years (1990–1993) and obtained a mean value of 0.141 and 0.122 for July and February, respectively, for three observation sites. In contrast, AVHRR albedos at this vegetation type are 0.142 in July and

0.143 in February, with spatial standard deviations of 0.020 and 0.036 in these two months, respectively. The AVHRR values in February during the rainy season may be biased high because of difficulties in obtaining samples that are not affected by subpixel cloudiness.

Both models show higher albedos than AVHRR data over broadleaf deciduous trees by 0.02 in BATS and 0.06 in LSM during February. Albedos for needleleaf evergreen trees are also in good agreement with LSM and BATS (higher by only 0.01 than the albedo of AVHRR). The albedos of needleleaf deciduous trees in both models match AVHRR data very well, with values around 0.137. Both models are biased high by about 0.02 over tundra. The short grass albedos of BATS match very closely those of AVHRR; LSM is high by 0.01 to 0.04. Tall grass albedos of both models are higher than that of AVHRR by over 0.02. Model-derived albedos for evergreen shrub are significantly lower compared to those of AVHRR, BATS from 0.01 to 0.03, and LSM from 0.03 to 0.07. For deciduous shrub, the albedos of AVHRR are close to BATS albedos, only slightly higher by 0.005, but are higher than those of LSM by over 0.04. Crop

albedos of both models are larger compared to those of AVHRR, by 0.02 to 0.04 for BATS and 0.01 to 0.02 for LSM.

5. Summary and conclusions

This study analyzes the albedo calculated by two land surface models and studies their seasonal variation at six specific land cover types. The differences between the albedos of the two models are caused by factors inherent to the dominant land cover type, such as the assigned vegetation albedo, or the vegetation fraction or LAI. Soil moisture differences are important for broadleaf evergreen trees. Soil color differences are a major factor in determining albedo for desert and semidesert regions. Finally, the model treatment of snow processes is crucial for tundra and needleleaf evergreen trees, where large differences are found between the two models.

A global albedo data set for February and July 1995, described by *Strugnell and Lucht* [2001], is used to evaluate model-calculated albedos. Large biases are found in desert and semidesert regions. Both models show albedos that are too high in winter when compared with the ground-measured albedo from BOREAS and with the AVHRR data. However, the satellite-derived surface albedos have been constructed to favor snow-free values and therefore do not realistically reflect the snow cover expected in high latitudes in winter. In addition, any particular year will show some anomalies in surface albedo related to other climate anomalies (e.g., surface temperatures and precipitation), and 1995 may have had some especially large such anomalies. However, we established that the use of the 1995 SSTs rather than climatological values for model boundary conditions changes the model albedos by much less than the discussed differences between model and AVHRR data.

The largest discrepancies between the model and the AVHRR albedos for snow-free surfaces are found in the desert and semidesert land cover types. On average, LSM values are about 0.29 and BATS 0.33, compared to a value of 0.26 for AVHRR. Because the models tend to give biases of similar magnitude but opposite signs in comparison with albedos inferred from ERBE, the present comparison alone is not convincing evidence that their desert albedos should be adjusted downward. However, the present cold biases in CCM3 simulations [Bonan, 1998], especially over North Africa, make it tempting to believe the AVHRR desert albedos.

In spite of such limitations the remotely sensed measurements provide good first guesses to modify parameters in models. For example, Bonan [1998] described CCM3 simulated desert temperatures that are 10 K lower than the climatology of *Legates and Willmott* [1990]. Some of this bias is probably a consequence of the high soil albedos [Bonan, 1998]. However, simply "tuning" surface albedos to obtain correct surface temperatures may obscure deficiencies in the representation

of physical processes within the land surface model and in its coupling to the atmospheric boundary layer. The satellite data may also be useful as a measure of the spatial heterogeneity of the surface and to constrain the land boundary conditions in other ways.

Acknowledgments. We thank the NCAR SCD, partly funded by the National Science Foundation, for supplying the required computational resources for the simulations used here. Funding for this study was provided by NASA EOS Interdisciplinary Scientific Research Program (UPN 428-81-22 and UPN 429-81-22). ANH was supported by the DOE Climate Change Prediction Program under grant PEPG-0398-ER-6206, and ZLY was supported under NASA grant NAG8-1520. C. Schaaf and N. Strugnell were supported by NASA under NAS5-31369 and by JPL under subcontract 960916/97. Two anonymous reviewers are thanked for helpful comments. M. Sanderson-Rae edited the manuscript.

References

- Anderson, E. A., *A Point Energy and Mass Balance Model of a Snow Cover*, 150 pp., Office of Hydrol., Natl. Weather Serv., Washington, D. C., 1976.
- Barker, H., and J. Davies, Surface albedo estimates from Nimbus-7 ERB data and a two-stream approximation of the radiative transfer equation, *J. Clim.*, **2**, 409–418, 1989.
- Bastable H. G., W. J. Shuttleworth, R. L. G. Dallarosa, G. Fisch, and C. A. Nobre, Observations of climate, albedo, and surface radiation over cleared and undisturbed Amazonian forest, *Int. J. Climatol.*, **13**, 783–796, 1993.
- Betts, A. K., and J. H. Ball, Albedo over the boreal forest, *J. Geophys. Res.*, **102**, 28,901–28,909, 1997.
- Bonan, G. B., A land surface model (LSM version 1.0) for ecological, hydrological, and atmospheric studies: Technical description and user's guide, *NCAR Tech. Note, NCAR/TN-417+STR*, 150 pp., Natl. Cent. Atmos. Res., Boulder, Colo., 1996.
- Bonan, G. B., The land surface climatology of the NCAR land surface model coupled to the NCAR Community Climate Model, *J. Clim.*, **11**, 1307–1326, 1998.
- Charney, J. G., W. J. Quirk, S. H. Chow, and J. Kornfield, A comparative study of the effects of albedo change on drought in semi-arid regions, *J. Atmos. Sci.*, **34**, 1366–1385, 1977.
- Clinton, M. R., Global land-surface albedo modeling, *Int. J. Climatol.*, **13**, 473–495, 1993.
- Csiszar, I., and G. Gutman, Mapping global land surface albedo from NOAA AVHRR, *J. Geophys. Res.*, **104**, 6215–6228, 1999.
- Culf, A. D., G. Fisch, and M. F. Hodnett, The albedo of Amazonian forest and ranch land, *J. Clim.*, **8**, 1544–1554, 1995.
- Dickinson, R. E., and B. Hanson, Vegetation-albedo feedbacks, in *Climate Processes and Climate Sensitivity*, *Geophys. Monogr.*, vol. 29, edited by J. E. Hanson and T. Takahashi, AGU, Washington, D. C., 1984.
- Dickinson, R. E., and A. Henderson-Sellers, Modeling tropical deforestation: A study of GCM land-surface parameterizations, *Q. J. R. Meteorol. Soc.*, **114**, 439–462, 1988.
- Dickinson, R. E., A. Henderson-Sellers, and P. J. Kennedy, Biosphere-Atmosphere Transfer Scheme (BATS) Version 1e as coupled to the NCAR Community Model, *NCAR Tech. Note, NCAR/TN-387+STR*, 72 pp., Natl. Cent. Atmos. Res., Boulder, Colo., 1993.
- Dirmeyer, P. A., and K. Shukla, Albedo as a moderator

- of climate response to tropical deforestation, *J. Geophys. Res.*, *99*, 20,863–20,877, 1994.
- Hahmann, A. N., and R. E. Dickinson, RCCM2/BATS model over tropical South America: Applications to tropical deforestation, *J. Clim.*, *10*, 1944–1964, 1997.
- Hahmann, A. N., and R. E. Dickinson, A fine-mesh land approach for general circulation models and its impact on regional climate, *J. Clim.*, *14*, 1634–1646, 2001.
- Legates, D. R., and C. J. Willmott, Mean seasonal and spatial variability in global surface air temperature, *Theor. Appl. Climatol.*, *41*, 11–21, 1990.
- Li, X., and A. H. Strahler, Geometric-optical bi-directional reflectance modeling of the discrete crown vegetation canopy: Effect of crown shape and mutual shadowing, *EEE Trans. Geosci. Remote Sens.*, *30*, 276–292, 1992.
- Li, Z., and L. Garand, Estimation of surface albedo from space: A parameterization for global application, *J. Geophys. Res.*, *99*, 8335–8350, 1994.
- Loveland, T. R., B. C. Reed, J. F. Brown, D. O. Ohlen, J. Zhu, L. Yang, and J. W. Merchant, Development of a global land cover characteristics database and IGBP DISCover from 1-km AVHRR data, *Int. J. Remote Sens.*, *21*, 1303–1330, 2000.
- Lucht, W., C. B. Schaaf, and A. H. Strahler, An algorithm for the retrieval of albedo from space using semiempirical BRDF models, *IEEE Trans. Geosci. Remote Sens.*, *38*, 977–998, 2000.
- Marshall, S. E., A physical parameterization of snow albedo for use in climate models, NCAR Coop. thesis, Natl. Cent. Atmos. Res., Boulder, Colo., 1989.
- Matthews, E., Global vegetation and land use: New high-resolution data bases for climate studies, *J. Clim. Appl. Meteorol.*, *22*, 474–487, 1983.
- Matthews, E., Atlas of archived vegetation, land-use and seasonal albedo database, *NASA Tech. Memo.*, pp. 86–199, 1985.
- Monteith, J. L., *Principles of Environmental Physics*, Edward Arnold, London, 1973.
- National Oceanic and Atmospheric Administration (NOAA), *Clim. Diagnostic Bull. 95/2*, Washington, D. C., 1995.
- Oguntoyinbo, J. S., Reflection coefficient of natural vegetation, crops and urban surfaces in Nigeria, *Q. J. R. Meteorol. Soc.*, *96*, 430–441, 1970.
- Olson, J. S., *Global Ecosystem Framework-Definitions*, internal report, 37 pp., U. S. Geol. Serv., EROS Data Cent., Sioux Falls, S. D., 1994.
- Olson, J. S., J. A. Watts, and L. J. Allison, Carbon in live vegetation of major world ecosystems, *US DOE Tech. Rep., DOE/NBB-0037, TR004*, U. S. Dept. of Energy, Washington, D. C., 152 pp., 1983.
- Pinker, R. T., O. E. Thompson, and T. F. Eck, The albedo of a tropical evergreen forest, *Q. J. R. Meteorol. Soc.*, *106*, 551–558, 1980.
- Rockwood, A. A., and S. K. Cox, Satellite-infrared surface albedo over Northwestern Africa, *J. Atmos. Sci.*, *35*, 513–522, 1978.
- Ross, J., *The Radiation Regime and Architecture of Plant Stands*, 392 pp., Dr. W. Junk, Norwell, Mass., 1981.
- Roujean, J.-L., M. Leroy, and P.-Y. Deschamps, A bidirectional reflectance model of the Earth's surface for the correction of remote sensing data, *J. Geophys. Res.*, *97*, 20,455–20,468, 1992.
- Sellers, P. J., Canopy reflectance, photosynthesis and transpiration, *Int. J. Remote Sens.*, *6*, 1335–1372, 1985.
- Shuttleworth W. J., et al., Observations of radiation exchange above and below Amazonian forest, *Q. J. R. Meteorol. Soc.*, *110*, 1163–1169, 1984.
- Strugnell, N., and W. Lucht, Continental-scale albedo inferred from AVHRR data, land cover class and field observations of typical BRDFs, *J. Clim.*, *14*, 1360–1376, 2001.
- Strugnell, N., W. Lucht, and C. Schaaf, A global albedo data set derived from AVHRR data for use in climate simulations, *Geophys. Res. Lett.*, *28*, 191–194, 2001.
- Tucker, C. J., J. R. G. Townshend, and T. E. Golf, African land-cover classification using satellite data, *Science*, *227*, 369–374, 1985.
- Vermote, E. F., N. El Saleous, C. O. Justice, Y. J. Kaufman, J. L. Privette, L. Temer, J. C. Roger, and D. Tanre, Atmospheric correction of visible to middle-infrared EOS-MODIS data over land surface: Background, operational algorithm and validation, *J. Geophys. Res.*, *102*, 17,131–17,141, 1997.
- Wanner, W., X. Li, and A. H. Strahler, On the derivation of kernels for kernel-driven models of bidirectional reflectance, *J. Geophys. Res.*, *100*, 21,077–21,090, 1995.
- Wiscombe, W. J., and S. G. Warren, A model for the spectral albedo of snow, I, Pure snow, *J. Atmos. Sci.*, *37*, 2712–2733, 1980.
- Xue, Y., and J. Shukla, The influence of land surface properties on Sahel climate, Part 1, Desertification, *J. Clim.*, *6*, 2232–2246, 1993.
- Yang, Z.-L., and G.-Y. Niu, Snow-climate interaction in NCAR CCM3, *Proceedings 15th Conference on Hydrology*, pp. 24–27, Am. Meteorol. Soc., Boston, Mass., 2000.
- Yang, Z.-L., R. E. Dickinson, A. Robock, and K. Y. Vinikov, Validation of the snow submodel of the Biosphere-Atmosphere Transfer Scheme with Russian snow cover and meteorological observational data, *J. Clim.*, *10*, 353–373, 1997.
- Yang, Z.-L., R. E. Dickinson, A. N. Hahmann, M. Shaikh, G.-Y. Niu, X. Gao, R. C. Bales, S. Sorooshian, and J. M. Jin, Simulation of snow mass and extent in global climate models, *Hydrol. Process.*, *13*, 2097–2113, 1999.

R. E. Dickinson, School of Earth and Atmospheric Sciences, Georgia Institute of Technology, Atlanta, GA 30332, USA.

A. N. Hahmann, X. Wei, and X. Zeng, Institute of Atmospheric Physics, 1118 E. 4th Street, University of Arizona, Tucson, AZ 85721-0081, USA.

(hahmann@atmo.arizona.edu)

C. B. Schaaf and N. Strugnell, Department of Geography and Center for Remote Sensing, Boston University, Boston, MA 02215, USA.

K. J. Schaudt, Department of Physics, 1118 E. 4th Street, University of Arizona, Tucson, AZ 85721-0081, USA.

Z.-L. Yang, Department of Hydrology and Water Resources, University of Arizona, Tucson, AZ 85721-0011, USA.

(Received August 25, 2000; revised April 16, 2001; accepted April 18, 2001.)